

Methane bursts as a trigger for intermittent lake-forming climates on post-Noachian Mars

Edwin S. Kite^{1,*}, Peter Gao^{2,3}, Colin Goldblatt⁴, Michael A. Mischna⁵, David P. Mayer^{1,6}, Yuk L. Yung⁶.

1. Department of Geophysical Sciences, University of Chicago, Chicago, IL 60637.
2. NASA Ames Research Center, Mountain View, CA 94035.
3. Astronomy Department, University of California, Berkeley, CA 94720.
4. School of Earth and Ocean Sciences, University of Victoria, Victoria BC, V8P 5C2, Canada.
5. Jet Propulsion Laboratory, Pasadena, CA 91109.
6. U.S. Geological Survey, Astrogeology Science Center, Flagstaff, AZ.
7. Division of Geological and Planetary Sciences, California Institute of Technology, Pasadena, CA 91125. *e-mail: kite@uchicago.edu.

Journal reference: *Nature Geoscience*, 10, 737–740 (2017) doi:10.1038/ngeo3033

Lakes existed on Mars later than 3.6 billion years ago, according to sedimentary evidence for deltaic deposition. The observed fluvio-lacustrine deposits suggest that individual lake-forming climates persisted for at least several thousand years (assuming dilute flow). But the lake watersheds' little-weathered soils indicate a largely dry climate history, with intermittent runoff events. Here we show that these observational constraints, while inconsistent with many previously-proposed triggers for lake-forming climates, are consistent with a methane burst scenario. In this scenario, chaotic transitions in mean obliquity drive latitudinal shifts in temperature and ice loading that destabilize methane clathrate. Using numerical simulations, we find that outgassed methane can build up to atmospheric levels sufficient for lake-forming climates, for past clathrate hydrate stability zone occupancy fractions >0.04. Such occupancy fractions are consistent with methane production by water-rock reactions due to hydrothermal circulation on early Mars. We further estimate that photochemical destruction of atmospheric methane curtails the duration of individual lake-forming climates to less than a million years, consistent with observations. We conclude that methane bursts represent a potential pathway for intermittent excursions to a warm, wet climate state on early Mars.

Runoff on Mars after ~3.6 Ga was uncommon and episodic. Episodes of runoff are recorded by deltas and fans. Fan/delta watershed mineralogy shows limited aqueous weathering, and watershed topography lacks the slope-area scaling expected for prolonged fluvial erosion. Thus, mineralogy and geomorphology suggest runoff

episodes were brief. Yet surprisingly, sediment and water mass balance calculations for $\lesssim 3.6$ Ga precipitation-fed paleolakes do not suggest a palimpsest of catastrophic events. To the contrary, runoff production of 0.1-1 mm/hr and lake lifetimes of >3 Kyr (assuming dilute flow) requires sustained, non-catastrophic cycling of lake-water (e.g. refs. 1-3) (Table S1). Catchments lack evidence for extensive leaching⁴, and retain mafic minerals such as olivine, which dissolves quickly in water (Methods). Furthermore, late-stage fluvial incision into delta and fan deposits is uncommon. In summary, individual lake-forming climates lasted >3 Kyr but shut down rapidly.

Drawing out the implications of intermittency data

To draw out the implications of the intermittency data, we use a conceptual model of catchment response to a ~ 3 Ga wet episode (Fig. 1a). Consistent with models (e.g. Mischna et al. 2013), we assume that snow falls in low-latitude catchments when obliquity (ϕ) $>40^\circ$. During a wet-climate anomaly, runoff from snowmelt transports sediment to build a fan/delta. This phase lasts $>(3-10)$ Kyr (the product of delta volume and water:sediment ratio, divided by the energy-limited lake evaporation rate)¹⁻³ (Table S1). During this phase, erosion may expose mafic minerals (e.g. olivine) in sediment-source regions (Fig. 1a). As climate cools, meltwater production is insufficient to transport sediment, but still wets the active-layer soil and so dissolves olivine. The duration of this phase cannot exceed the olivine-dissolution lifetime, $\sim 10^6$ yr (refs. 5-6).

Hypotheses for the trigger of lake-forming climates should match constraints on the intermittency and cadence of those climates. Many existing hypotheses for the trigger of lake-forming climates underpredict lake lifetime (Fig. 1b). Individual volcanic eruptions only permit wet events of at most hundreds of years duration^{7,8}. Models of ~ 3 Ga asteroid impacts predict <0.1 yr runoff⁹. Alternatively, a H_2 - CO_2 greenhouse requires >0.15 Myr to remove H_2 at the diffusion-limited rate¹⁰; this is marginally consistent with data, but requires a brief $>10^7$ km³ pulse of late-stage volcanism (or clathrate release; ref. 11) to provide H_2 . Recently, limit cycles involving rapid deglaciation and rapid carbonate formation have been proposed to explain >3.6 Ga lake-forming climates¹². Such a limit cycle is implausible for $\lesssim 3.6$ Ga lakes because post-Noachian soil thicknesses and erosion rates provide insufficient cations for rapid weathering drawdown of the atmosphere¹³, and because the hypothesized carbonates would reside near the modern surface in conflict with spectroscopic constraints¹⁴.

Methane bursts as a trigger for intermittent lake-forming climates

An alternative trigger for lake-forming climates is chaotic transitions in Mars' mean obliquity. These transitions are large ($10-20^\circ$), brief (often $\lesssim 10^7$ yr), and infrequent: transported to a random point in Mars' history, one would expect to find oneself in a

0.5 Gyr-long interval of continuously high (or low) Myr-mean ϕ (Fig. 2). The brevity and large time interval of mean- ϕ transitions matches the brevity and rarity of lake-forming climates. Moreover, mean- ϕ transitions cause latitudinal shifts in temperature, which destabilizes ice/snow (e.g., ref. 15). Thus ϕ shifts can increase the amount of water in the atmosphere, favor cirrus-cloud warming¹⁶, and prime surface snowpack for runoff¹⁵.

During a large shift in mean ϕ , the subsurface will undergo correspondingly large changes in pressure (as surface ice and ground ice migrate) and temperature. At some latitudes this will destabilize CH₄-clathrate, yielding CH₄ gas¹⁷. CH₄-clathrate breakdown involves a >14% reduction in solid volume, and we assume fractures allow methane gas released at $\leq 100\text{m}$ depth to reach the surface in $\ll 10^4$ yr (ref. 18). In our scenario, the ultimate source of CH₄ is hydrothermal circulation (e.g. serpentinization) early in Mars history (e.g. ref. 19). The CH₄-production stoichiometric upper limit (for hydrothermal reactions) is $>10^4 \times$ greater than the amount needed to shift planetary climate (Methods). Methane-saturated fluids will deposit clathrate on approach to a cold surface. As Mars cools, the hydrate stability zone (HSZ) expands. Methane will diffuse out of the HSZ only slowly, but once destabilized, CH₄-clathrate dissociates geologically quickly²⁰.

Mean- ϕ transitions can lead to build-up of millibars of methane in Mars' atmosphere. To show this, we used calculations of Mars' spin and orbit ²¹, output from a Global Climate Model¹⁵, a parameterization of the greenhouse effect of CH₄ (ref. 22), and a photochemical model of CH₄ destruction²³, in order to drive a model of CH₄-clathrate stability in Mars' subsurface (Methods). We used mobile ice+dust overburden of ~ 40 m thickness²⁴. The fraction f of the HSZ that is occupied by hydrate is a free parameter. Example output is shown in Fig. 3. Following model spinup, little happens for ~ 0.2 Gyr. CH₄ released to the atmosphere during quasi-periodic orbital change¹⁷ is maintained below radiatively significant levels by UV photolysis²⁵. Then, a mean- ϕ shift occurs, swiftly destabilizing CH₄-clathrate (Fig. 3). CH₄ release temporarily overwhelms photolysis by UV (we use a ~ 3.0 Ga UV flux; ref. 26); CH₄ accumulates in the atmosphere. Our photochemical modeling (Methods) shows that the Mars atmosphere CH₄-enrichment episode duration is set by UV photon supply, the CH₄ /CO₂ ratio, and other photochemical effects, and is 10^5 - 10^6 years. This duration allows for multiple orbitally-paced pulses of runoff in a given lake basin, consistent with data³, and satisfies the lake duration constraint. CH₄ peaks early in the episode and declines gradually. Because the CH₄-clathrate reservoir is recharged slowly if at all, the CH₄-burst mechanism also satisfies the olivine-dissolution constraint.

$\geq 1\%$ methane can switch the Mars system from zero meltwater production to a lake-forming climate. 1% of CH₄ added to a ~ 1 bar CO₂ atmosphere in a clear-sky radiative-convective calculation boosts temperature by 6K (ref. 22). These corresponding CO₂ pressures are consistent with proxy data²⁷⁻²⁸, assuming lakes

were ice-covered. The boosted temperatures are high enough for perennial ice-covered lakes to form²⁹⁻³⁰. In our calculations $\text{CH}_4/\text{CO}_2 \leq 0.1$, so photochemical production of C_2H_6 is minor and anti-greenhouse haze cannot form. However, abiotic hydrothermal reactions produce C_2H_6 with 10^{-3} - 10^{-1} the efficiency of CH_4 (ref. 31), and C_2H_6 partitions readily into clathrate¹⁸. The greenhouse effect of even 1% $\text{C}_2\text{H}_6/\text{CH}_4$ would be radiatively significant³²⁻³³. Although CH_4 photolysis yields H_2 , the additional warming is modest. The likely presence of clouds would moderate total warming, but only by 14-30% (ref. 34).

Methane bursts link subsurface and surface hydrology

CH_4 -induced surface warming swiftly destabilizes CH_4 -clathrate at greater depth, which releases additional CH_4 . This CH_4 -release feedback greatly increases total CH_4 warming for $f > 0.04$; for $f < 0.04$, it is difficult to trigger a lake-forming episode. In addition, during a lake-forming event, lake-bottom temperature rises to $>273\text{K}$ even for ice-covered lakes. This warming destabilizes sub-lake clathrates. Subsequent CH_4 degassing (e.g. via mud volcanoes) adds to atmospheric CH_4 . The largest proposed paleolake on Mars is 10^6 km^2 (ref. 35) and seas as large as $2.3 \times 10^7 \text{ km}^2$ have been suggested (e.g. ref. 36). Because the lake-bottom warming is long-lived, sub-lake pore ice melts to open permeable conduits (through-taliks) to the deep hydrosphere.

There are other mechanisms by which mean- ϕ transitions could drive lake formation by linking surface and subsurface hydrology³⁷. For example, ice unloading could promote hydrofracture discharge of overpressured aquifers. Clathrate decomposition, e.g. driven by ϕ changes, might directly trigger outflow channels³⁷, and chaos terrain formation could also release CH_4 : individual chaos-terrains have volumes up to 10^5 km^3 . Chaos terrain formation could be associated with shallow magmatic intrusions, which might themselves destabilize CH_4 .

Lake-forming climates in the context of Mars history

Because widely-spaced CH_4 bursts are possible, we hypothesize that the $\sim 3 \text{ Ga}$ lake-forming climate may be a late echo of the more-intense $\sim 4 \text{ Ga}$ climate upswing that cut valley networks and filled inland seas³⁸. For example, atmospheric collapse could drive ice sheets from highlands to poles³⁹, depressurizing sub-ice clathrate. Conversely, >5 widely-separated lake episodes would be inexplicable by CH_4 bursts alone.

In our model, surface climate $\lesssim 3.6 \text{ Gyr}$ ago is driven by CH_4 produced during earlier water-rock reactions¹¹. $>3.6 \text{ Ga}$ serpentinization has been documented from orbit⁴⁰, and data suggest cool mid-crustal temperatures that are consistent with pervasive hydrothermal circulation⁴¹⁻⁴². The abundant CH_4 predicted by our model could be tested with better constraints on permeability, alteration extent, and fluid chemistry in ancient deep aquifers⁴³. Furthermore, the CH_4 -clathrate reservoir on Mars should never

completely vanish. Present-day CH₄ outgassing is predicted⁴⁴. CH₄ outgassing has been reported from ground-based and rover instruments (e.g. ref. 45). Our model indicates that (after many chaotic-obliquity shifts) ancient clathrate should be closest to the surface in dusty longitudes at 30-50°N. The ExoMars orbiter may decisively test modern outgassing⁴⁶.

Our model of uncommonly wet climates on post-3.6 Ga Mars does not account for the lesser amounts of liquid water needed to explain the prolonged accumulation of sedimentary rocks near Mars' equator (e.g. 47-48). While CH₄ bursts can explain the cadence of lake-forming climates, the problem of accounting for these sedimentary rocks remains open^{39,49}.

References.

1. Irwin, R.P., Lewis, K.W., Howard, A.D., Grant, J.A. Paleohydrology of Eberswalde crater, Mars. *Geomorphology* **240**, 83-101 (2015).
2. Palucis, M.C., et al.. Sequence and relative timing of large lakes in Gale crater (Mars) after the formation of Mount Sharp. *J. Geophys. Res.- Planets* **121**, 472-496 (2016).
3. Williams, R.M.E., Weitz, C.M. Reconstructing the aqueous history within the southwestern Melas basin, Mars: Clues from stratigraphic and morphometric analyses of fans. *Icarus* **242**, 19-37 (2014).
4. Milliken, R.E., Bish, D.L. Sources and sinks of clay minerals on Mars. *Phil. Mag.* **90**, 2293-2308 (2010).
5. Olsen, A.A., & Rimstidt, J.D., Using a mineral lifetime diagram to evaluate the persistence of olivine on Mars, *Am. Mineral.* **92**, 598-602 (2007).
6. Stopar, J.D., Taylor, G.J., Hamilton, V.E., Browning, L. Kinetic model of olivine dissolution and extent of aqueous alteration on mars. *Geochim. et Cosmochim. Acta* **70**, 6136-6152 (2006).
7. Halevy, I., Head, J.W., III, Episodic warming of early Mars by punctuated volcanism. *Nature Geoscience* **7**, 865-868 (2014).
8. Kerber, L., Forget, F., Wordsworth, R. Sulfur in the early martian atmosphere revisited: Experiments with a 3-D Global Climate Model. *Icarus* **261**, 133-148 (2015).
9. Segura, T.L., Zahnle, K., Toon, O.B., McKay, C.P. pp. 417-437 in Mackwell, S., et al. (Eds). *Comparative Climatology of Terrestrial Planets*, University of Arizona Press (2013).

10. Batalha, N.; Domagal-Goldman, S.D.; Ramirez, R.; Kasting, J.F. Testing the early Mars H₂-CO₂ greenhouse hypothesis with a 1-D photochemical model, *Icarus* **258**, 337-349 (2015).
11. Chassefière, E., Lasue, J., Langlais, B., Quesnel, Y. Early Mars Serpentinization Derived CH₄ Reservoirs and H₂ Induced Warming. *Meteoritics & Planetary Science* **51**, 2234–2245 (2016).
12. Batalha, N.; Kopparapu, R. K.; Haqq-Misra, J.; Kasting, J. F. Climate cycling on early Mars caused by the carbonate-silicate cycle, *Earth Planet. Science Lett.* **455**, 7-13 (2016).
13. Edwards, C.S.; Ehlmann, B.L., Carbon sequestration on Mars. *Geology* **43**, 863-866 (2015).
14. Ehlmann, B.L.; Edwards, C.S., Mineralogy of the Martian Surface, *Ann. Rev. Earth Planet. Sci.* **42**, 291-315 (2014).
15. Mischna, M.A., Baker, V., Milliken, R., Richardson, M., Lee, C. Effects of obliquity and water vapor/trace gas greenhouses in the early martian climate. *J. Geophys. Res. - Planets* **118**, 560-576 (2013).
16. Urata, R.A., Toon, O.B. Simulations of the martian hydrologic cycle with a general circulation model: Implications for the ancient martian climate. *Icarus* **226**, 229-250 (2013).
17. Prieto-Ballesteros, O., et al. Interglacial clathrate destabilization on Mars: Possible contributing source of its atmospheric methane. *Geology* **34**, 149 (2006).
18. Sloan, E.D., & Koh, C.A, Clathrate Hydrates of Natural Gases (3rd Edition), CRC Press (2008).
19. Lyons, J.R., Manning, C., Nimmo, F. Formation of methane on Mars by fluid-rock interaction in the crust. *Geophys. Res. Lett.* **32**, L13201 (2005).
20. Root, M.J., Elwood Madden, M.E. Potential effects of obliquity change on gas hydrate stability zones on Mars. *Icarus* **218**, 534-544 (2012)
21. Kite, E.S.; et al., Stratigraphy of Aeolis Dorsa, Mars: Stratigraphic context of the great river deposits. *Icarus* **253**, 223-242 (2015).
22. Wordsworth, R., et al., Transient reducing greenhouse warming on early Mars, *Geophys. Res. Lett.* **44**, 665-671 (2017).

23. Nair, H.; Summers, M.E.; Miller, C.E.; Yung, Y.L., 2005, Isotopic fractionation of methane in the martian atmosphere, *Icarus* **175**, 32-35.
24. Kadish, S.J., Head, J.W., Barlow, N.G. Pedestal crater heights on Mars: A proxy for the thicknesses of past, ice-rich, Amazonian deposits. *Icarus* **210**, 92-101 (2010).
25. Krasnopolsky, V.A., Maillard, J.P., Owen, T.C. Detection of methane in the martian atmosphere: evidence for life? *Icarus* **172**, 537-547 (2004).
26. Claire, M.W, et al., The Evolution of Solar Flux from 0.1 nm to 160 μm , *Astrophys. J.* **757**, article id. 95, 12 pp. (2012).
27. Kite, E.S.; Williams, J.-P.; Lucas, A.; Aharonson, O., Low palaeopressure of the martian atmosphere estimated from the size distribution of ancient craters. *Nature Geoscience* **7**, 335-339 (2014).
28. Bristow, T.F., et al., Low Hesperian pCO_2 constrained from in situ mineralogical analysis at Gale Crater, Mars, *Proc. Natl. Acad. Sci.* **114**, 2166-2170 (2017).
29. Doran, P.T. et al., Valley floor climate observations from the McMurdo dry valleys, Antarctica, 1986-2000, *J. Geophys. Res.* **107**, D24, pp. ACL 13-1-ACL 13-12, (2002).
30. Le Deit, L., et al., Sequence of infilling events in Gale Crater, Mars: Results from morphology, stratigraphy, and mineralogy. *J. Geophys. Res. – Planets* **118**, 2439–2473 (2013).
31. Etiope, G., Sherwood Lollar, B. 2013. Abiotic Methane on Earth. *Rev. Geophys.* **51**, 276-299.
32. Haqq-Misra, J.D., Domagal-Goldman, S.D., Kasting, P.J., Kasting, J.F., A Revised, Hazy Methane Greenhouse for the Archean Earth. *Astrobiology* **8**, 1127-1137 (2008).
33. Byrne, B., Goldblatt, C. Radiative forcings for 28 potential Archean greenhouse gases. *Clim. Past* **10**, 1779-1801 (2014).
34. Goldblatt, C.; Zahnle, K. J., Clouds and the Faint Young Sun Paradox, *Clim. Past* **7**, 1, 203-220 (2011).
35. Michalski, J.R., Noe Dobrea, E.Z., Niles, P.B., & Cuadros, J., Ancient hydrothermal seafloor deposits in Eridania basin on Mars. *Nature Communications* **8**, article number: 15978 (2017).

36. Rodriguez, J. Alexis P.; et al., 2016, Tsunami waves extensively resurfaced the shorelines of an early Martian ocean, *Nature Scientific Reports* **6**, id. 25106 (2016).
37. Baker, V.R., Strom, R.G., Gulick, V.C., Kargel, J.S., Komatsu, G. Ancient oceans, ice sheets and the hydrological cycle on Mars. *Nature* **352**, 589-594 (1991).
38. Irwin, R.; Howard, A.; Craddock, R.; Moore, J., An intense terminal epoch of widespread fluvial activity on early Mars: 2. Increased runoff and paleolake development, *J. Geophys. Res.* **110**, E12S15 (2005).
39. Wordsworth, R.; Kerber, L.; Pierrehumbert, R.; Forget, F.; Head, J.W., 2015, Comparison of warm and wet and cold and icy scenarios for early Mars in a 3-D climate model, *J. Geophys. Res. - Planets* **120**, 1201-1219 (2015).
40. Ehlmann, B.L., Mustard, J.F., Murchie, S.L. Geologic setting of serpentine deposits on Mars. *Geophys. Res. Lett.* **37**, L06201 (2010).
41. Parmentier, E. M.; Zuber, M. T., Early evolution of Mars with mantle compositional stratification or hydrothermal crustal cooling. *J. Geophys. Res. - Planets* **112**, CiteID E02007 (2007)
42. Sun, V. Z., and R. E. Milliken, Ancient and recent clay formation on Mars as revealed from a global survey of hydrous minerals in crater central peaks, *J. Geophys. Res. Planets* **120**, 2293–2332 (2015).
43. Saper, L., Mustard, J.F. 2013. Extensive linear ridge networks in Nili Fossae and Nilosyrtris, Mars: implications for fluid flow in the ancient crust, *Geophys. Res. Lett.* **40**, 245-249.
44. Chassefière, E., Leblanc, F. Methane release and the carbon cycle on Mars. *Planet. Space Sci.* **59**, 207-217 (2011).
45. Webster, C.R., et al. Mars methane detection and variability at Gale crater. *Science* **347**, 415-417 (2015).
46. Vandaele, A.C., et al., Science objectives and performances of NOMAD, a spectrometer suite for the ExoMars TGO mission. *Planet. and Space Sci.* **119**, 233-249 (2015).
47. Malin, M.C., Edgett, K.S. Sedimentary Rocks of Early Mars. *Science* **290**, 1927-1937 (2000).
48. Fairén, A.G.; Davila, A.F.; Gago-Duport, L.; Amils, R.; McKay, C.P., Stability against freezing of aqueous solutions on early Mars, *Nature* **459**, 7245, 401-404 (2009).

49. Kite, E.S., Halevy, I., Kahre, M.A., Wolff, M.J., Manga, M. Seasonal melting and the formation of sedimentary rocks on Mars, with predictions for the Gale Crater mound. *Icarus* **223**, 181-210 (2013).

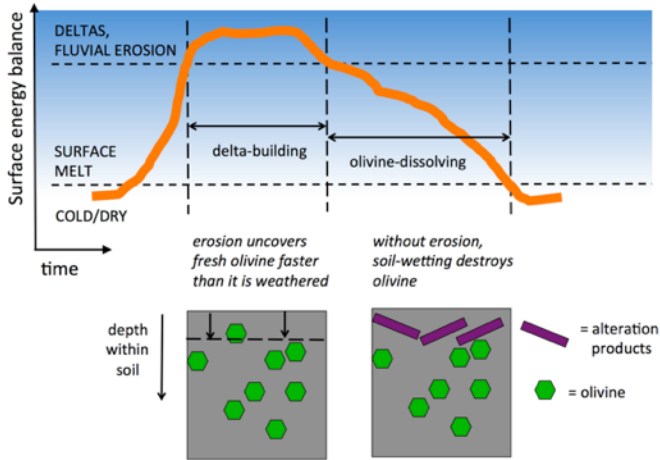
Acknowledgements. We are grateful for input from D.E. Archer, J.C. Armstrong, B.L. Ehlmann, V.E. Hamilton, A.D. Howard, R.P. Irwin III, M.C. Palucis, D. Stolper, R.M.E. Williams, and R. Wordsworth. We thank J.F. Kasting and A.G. Fairén for useful reviews. Part of the research was carried out at the Jet Propulsion Laboratory, California Institute of Technology, under a contract with the National Aeronautics and Space Administration. We acknowledge the University of Chicago's Research Computing Center and financial support from NASA (NNX16AG55G, NNX15AM49G).

Author contributions. E.S.K. designed research; M.M., Y.Y., and D.P.M. contributed new models, model output, and analyses; E.S.K., C.Z.G., and P.G. carried out research; and E.S.K. wrote the paper.

Additional information. Correspondence and requests for materials should be addressed to E.S.K. (kite@uchicago.edu)

Competing financial interests. The authors declare that they have no competing financial interests.

(a)



(b)

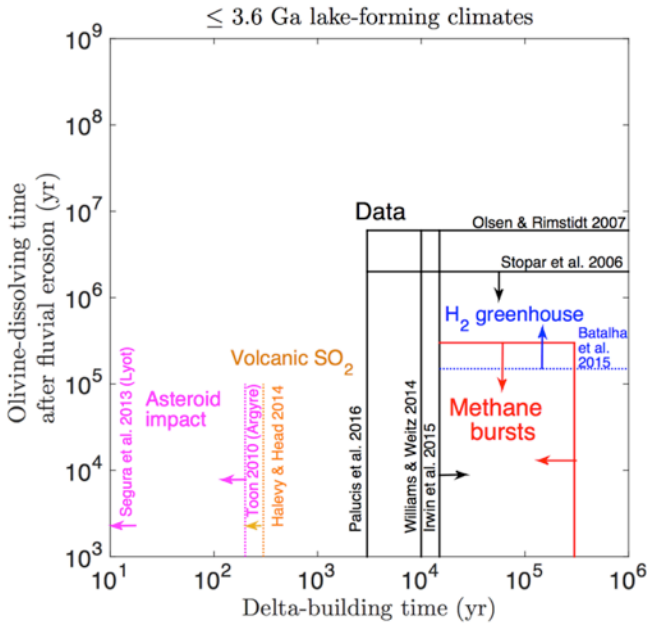


Fig. 1. Geologic constraints on the duration and shutdown-time of lake-forming climates. (a) Schematic showing how the delta-building timescale and the olivine-preservation timescale constrain duration and shutdown-time for a lake-forming climate episode. Olivine constrains soil-wetting after fluvial erosion ceases. (b) Geologic constraints (black lines) compared to models for the trigger mechanism of lake-forming climates (colored lines).

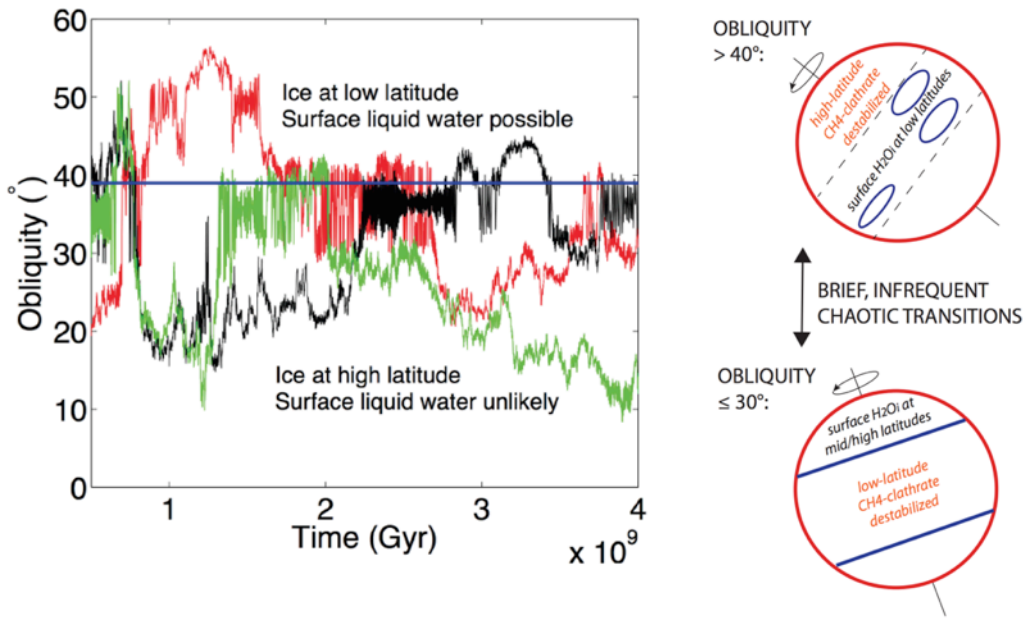


Fig. 2. Range of obliquity trajectories possible for Mars, and their likely climate effects. *Left:* Examples of possible, equally-likely, orbital histories for Mars. *Right:* Schematic showing effect of obliquity change on surface-ice distribution.

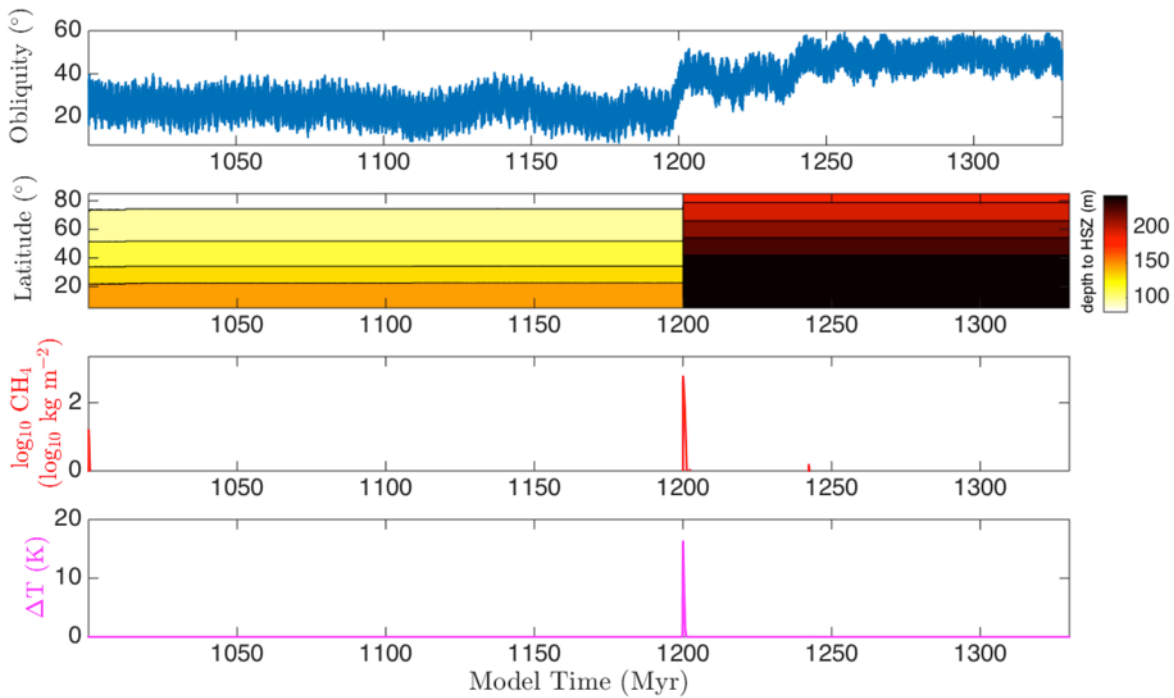


Fig. 3. Triggering of a CH₄-enabled lake-forming climate on Mars. Model time is arbitrary. (a) Example obliquity forcing (preceded by 0.3 Gyr of continuously

low obliquity). (b) Depth to the top of the clathrate-hydrate stability zone. Darkening denotes clathrate destabilization. (c) Atmospheric CH₄ column mass ($f = 0.045$). (d) Temperature change (from parameterization of Wordsworth et al. 2017). Temperature change is sufficient to produce an Antarctic-Dry-Valleys like climate. Lake-forming event lasts ~300 Kyr (Fig. S5a).

Methods.

Geologic Synthesis.

For many low-latitude fluviolacustrine deposits on Mars, geologic data indicate mid-Hesperian to Early Amazonian age^{1-3,50-57}. This corresponds⁵⁸ to ~3 Ga (or ~2 Ga using an alternative chronology⁵⁹). These deposits postdate the ~3.8 Ga highland valley networks of Mars⁵⁰, which are also hydrologically distinct from the younger fluviolacustrine deposits⁶⁰. Published data are consistent with the globally-distributed deposits having been caused by 1-2 intervals of delta-building. The water source for the features considered in this paper was precipitation (rain or snowmelt). Precipitation is indicated by spatially clustered watersheds with channels extending near ridgelines⁶¹. Snowmelt is a reasonable hypothesis for ~3 Ga deposits, although the reasoning set out in this paper does not rule out rainfall. Other ~3 Ga paleochannels and fluvial deposits (not considered here) are more ambiguous, and might be formed either by precipitation runoff⁶²⁻⁶³ or by localized water sources⁶⁴⁻⁶⁶.

The delta-forming duration τ_1 (duration of fluvial sediment transport) must exceed

$$\tau_1 > V_d(V_w/V_s)/E A_p \quad (1)$$

where V_d (m³) is measured delta volume, V_w/V_s is water:sediment ratio, E (m yr⁻¹) is the sum of evaporation rate (constrained by energy balance) and infiltration rate, and A_p (m²) is lake area¹⁻² (Table S1). Energy balance limits evaporation rate to <1 m yr⁻¹, and long-term average infiltration rate is likely small¹. Deposit morphology suggests dilute flows (debris-flow deposits are less common⁶⁷). Most authors therefore assume a dilute V_w/V_s ratio $\geq 10^3$, similar to Earth data⁶⁸. Long minimum lake lifetimes inferred from delta volumes (Table S1) are consistent with minimum runoff durations calculated from the energy-balance limit on snowmelt runoff production⁴⁹ combined with alluvial-fan volumes⁶⁷. Because water demands (column meters) of both deltas and alluvial-fans exceed the plausible thickness of preexisting snowpack, precipitation recharge of water source areas must have occurred during the wet event (i.e., a hydrologic cycle)^{1,67}.

Assuming runoff from snowmelt, runoff rate is directly related to surface energy balance. The surface energy balance difference J (W/m²) between the energetic threshold for soil wetting (no runoff), and the same threshold for fluvial sediment transport, is

$$J = \rho L(Q/A + I + E_e) \quad (2)$$

where ρ is liquid water density (1000 kg m^{-3}), L is latent heat of melting snow/ice (334 kJ kg^{-1}), Q is river paleodischarge ($\text{m}^3 \text{ s}^{-1}$), A is drainage area in m^2 (Q/A is “runoff production”), I is infiltration rate (mm hr^{-1}), and E_e is excess evaporation (mm hr^{-1}). A lower bound on J is obtained by setting I and E_e to zero; then $J = \rho L Q/A$. For $\lesssim 3.6$ Ga precipitation-fed channels, Q/A is estimated as $\sim 0.1\text{--}0.2 \text{ mm hr}^{-1}$ for Saheki⁶⁹, $0.03 - 0.4 \text{ mm hr}^{-1}$ for Peace Vallis⁷⁰, and $0.1\text{--}0.3 \text{ mm hr}^{-1}$ for Eberswalde¹. Taking 0.2 mm hr^{-1} as representative, $J = 20 \text{ W m}^{-2}$. These modest runoff requirements are consistent with an Antarctic-Dry-Valleys-like climate. An Antarctic-Dry-Valleys-like climate permits large lakes²⁹⁻³⁰.

We use olivine persistence as a constraint on the duration of soil-wetting climates (Fig. 1). Olivine is present in many Mars delta and alluvial-fan watersheds. Specifically, (1) Observatoire pour la Minéralogie, l'Eau, les Glaces et l'Activité (OMEGA) shows olivine⁷⁴ in some alluvial fan watersheds. (2) Thermal Emission Spectrometer (TES) data shows widespread olivine⁷⁵ including in alluvial fan watersheds. (3) Thermal Emission Imaging System (THEMIS) decorrelation stretches indicate olivine⁷⁶ in alluvial fan watersheds. (4) The Compact Reconnaissance Imaging Spectrometer for Mars (CRISM) OLINDEX3 parameter, which was designed as an indicator of olivine⁷⁷, shows high values in many alluvial fan watersheds. CRISM olivine detections in alluvial-fan watersheds include Robert Sharp crater⁷⁸ and Saheki (Fig. S1). Olivine persistence sets an upper limit on the duration of soil wetting by olivine-dissolving fluids. Olivine-dissolution data indicate olivine lifetimes $<(2\text{--}6) \text{ Myr}$ for $T \sim 278 \text{ K}$, for a pH corresponding to pure water pH equilibrated with 60 mbar CO_2 , and including a $100\times$ lab-to-field correction⁵⁻⁶. Thicker atmospheres, as required for most warming mechanisms, give lower pH and thus shorter lifetimes. However, buffering by rock dissolution increases pH and thus olivine lifetimes⁷⁹. Some calculations⁸⁰ give olivine lifetimes in fluids at Mars' surface as short as 10 yr . Short olivine-inferred water durations are consistent with short water durations inferred from (1) persistence of hydrated amorphous silica⁸¹, (2) commingling of unaltered olivine with sulfates in the Peace-class rocks at Gusev⁸², (3) persistence of jarosite⁸³, and (4) near-isochemical alteration of Bradbury group materials at Gale crater⁸⁴, among other methods. We assume that infiltrated water is present in soil throughout a wet season. This is reasonable because runoff generation from snowpack is extremely difficult unless snowpack reaches thermal maturity. Thermal maturity requires that average temperature during the warm month is near freezing⁸⁵. Additionally, infiltration, and latent heat release, protect water from complete freezing.

Although we focus on $\lesssim 3.6$ Ga lake-forming climate(s) in this study, the ~ 3.8 Ga lake-forming climate is also characterized by a relatively short-lived interval of intense fluvial sediment transport^{38,71-72} (see also ref. 73).

Our model includes a H_2O ice overburden that shifts with obliquity. Snow accumulation at latitude $<45^\circ$ at $\varphi > 40^\circ$ is supported by all Mars climate models^{15,39,49,86}.

Snow accumulation at latitude $<45^\circ$ at $\varphi > 40^\circ$ is also supported by observations of equatorial relict ice and glacial moraines⁸⁶. This latitudinal shift in snow distribution is caused by the increase in polar summer insolation at high obliquity. At high atmospheric pressure, snow/ice may be present at low latitudes regardless of φ , but water ice stability patterns still show latitudinal shifts³⁹ with φ . Laterally-extensive midlatitude volatile-rich layers that migrate under φ control were ~ 32 m thick based on relict Amazonian deposits⁸⁷, or (44 ± 23) m thick based on pedestal craters²⁴.

Assessment of previously-proposed trigger mechanisms.

- Volcanic SO₂: The SO₂-greenhouse model of ref. 7 predicts wet events of duration ~ 30 yr. This hypothesis struggles to match minimum lake-lifetime constraints, and SO₂-outgassing may in fact induce net cooling⁸.
- Climate change triggered by impact energy: Impact-triggered models for post-3.6 Ga wet climates must satisfy the geologic constraint of modest precipitation-sourced erosional modification of the six largest post-3.6 Ga craters on Mars⁸⁸. Ref. 16 proposes a metastable impact-triggered wet climate sustained by cloud forcing. Such a climate can sustain temperatures above 273K on annual average, but only with unrealistic total cloud cover⁸⁹. However, the model could generate seasonal melting with more realistic cloud-cover assumptions⁸⁹. Ref. 9 states that a metastable warm/wet climate can be attained from the impact of an 8 km-radius asteroid. Their maps do not show rain at the impact location itself, which is intriguingly consistent with post-3.6 Ga Mars data⁸⁸.
- Impact delivery of volatiles: Comets have $\sim 1\%$ CH₄ (ref 90.) One of the largest impact craters on Mars with age < 3.6 Ga is Lyot (ref. 88). Supposing Lyot to have been formed by a comet, the impact would have delivered < 0.01 mbar CH₄ (radiatively negligible).

Obliquity Simulations.

Mars obliquity (φ) is quasi-periodic on $< 10^6$ yr timescales but chaotic on $\geq 10^8$ yr timescales, ranging from $0-70^\circ$ (ref. 91). These large changes have correspondingly large effects on climate¹⁵. To generate realistic possible φ histories for ~ 3 Ga Mars, we first generated an ensemble of solar system simulations using the mercury6 N-body code⁹². We added φ /precession tracks in post-processing using (ref. 93). We generated randomness by shifting Mars's initial position, and by randomly selecting initial obliquities from the probability distribution functions of ref. 91. After the tracks have diverged from their initial conditions, each track (and each time interval of a given track) is an equally good estimate of ~ 3 Ga Mars behavior. Our obliquity runs show chaotic transitions⁹³ in mean φ . Transitions are separated by long periods during which mean φ does not vary greatly, consistent with previous work⁹⁴⁻⁹⁵. Our eccentricity

pdf agrees with that of ref. 91. Our ϕ pdf is unimodal, peaking at $\sim 40^\circ$, and with a shape close to that of ref. 91.

Surface Temperature Modeling.

We calculate surface temperature as a function of obliquity, latitude, CO₂ partial pressure, and CH₄ partial pressure. Our starting point is a grid of output from 20 runs of a CO₂ only GCM (derived from ref. 15), which were carried out assuming a solar luminosity 75% that of today's Sun, pCO₂ = {6, 60, 600, 1200} mbar, and ϕ = {15°, 25°, 35°, 45°, 60°}. We zonally-average and time-average the surface temperatures. We adjust results upwards by a fixed amount to match the results⁹⁶ of the LMD GCM, because the LMD GCM includes cloud and H₂O(v) effects that are absent in our GCMs. The LMD GCM predicts equatorial, datum-elevation, CH₄-free temperatures of ~ 245 K. For a given pCO₂, we interpolate in the grid of adjusted GCM results using our obliquity tracks to interpolate the surface temperature as a function of time and latitude. (The effects of varying eccentricity and longitude of perihelion are neglected, which has the indirect effect of stabilizing clathrate at low latitude.) These CH₄-absent temperatures drive initial CH₄ destabilization. After non-negligible CH₄ has entered the atmosphere, we add a uniform temperature offset to take account of CH₄-CO₂ collision-induced absorption²². This calculation includes the surface-cooling effect associated with the absorption of near-infrared sunlight by methane²². Our simple approach to calculating greenhouse forcing is appropriate for this study, because our goal is to explain runoff intermittency (not absolute temperature, not latitudinal gradients, not the existence of runoff).

Clathrate Modeling.

Charge-up. Early Mars had active magmatism, initially high geothermal heat flow, likely a large water inventory⁹⁷, and a basaltic/ultramafic crust. Therefore, the amount of CH₄ produced by serpentinization early in Mars history is potentially very large⁹⁸⁻⁹⁹. Whether this CH₄-production potential was realized depends on details of catalyst distribution and crustal permeability, which are poorly known even for Earth. Our CH₄-burst scenario requires no more than 0.0001× of the stoichiometric CH₄-production upper limit. Mars meteorites have $\sim(15-20)$ wt% FeO_T, i.e. 10-13 wt% Fe. Most of the Fe in the upper crust has FeO oxidation state. Assuming 1 electron per oxidized Fe, the CH₄-production upper limit is 7% of the mass of the Fe. Multiplying by an assumed mid-crustal alteration zone thickness of 5 km and density 3000 kg/m³ yields an electron-based stoichiometric upper limit of $\sim 10^2$ bars. In practice, the limit to CH₄-production would more likely be set by C availability. Mars crust production was extended over a long period including times during which the surface would have been cold. Therefore, CH₄ produced by water-rock reactions (for example by serpentinization and Fischer-Tropsch Type reactions; refs. 30,100) would have been trapped on approach to the cooling surface (e.g. beneath ice sheets or primordial seas) as clathrate (Fig. S3). CH₄ accumulates in $\sim 10^7$ yr by

cycling of CH₄-saturated water through the Hydrate Stability Zone (HSZ), or more quickly by bubble exsolution¹⁰¹. The fraction of HSZ volume that is occupied by clathrate (f in our model) must be divided by porosity to obtain the fraction of pore space that is occupied by clathrate. We assume a porosity of 0.3 (Lunar porosity is ~ 0.25)¹⁰². The extent to which pore space is filled on Mars by abiotic methane clathrate is unknown¹⁰³; on Earth biogenic methane clathrate fills $\sim 3\%$ of available pore space¹⁰⁴.

Release. CH₄ trapped in clathrate is retained for up to Gyr. Ref. 105 cites theoretical calculations¹⁰⁶ for which the diffusivity of CH₄ in the clathrate lattice (D_{CH_4}) is given by

$$D_{\text{CH}_4}(T) = 0.0028 \times X_{\text{CH}_4} \exp(-6.042 \times 10^{-13} / kT) \text{ cm}^2 \text{ s}^{-1} \quad (3)$$

where k is Boltzmann's constant. Setting $X_{\text{CH}_4} = 0.03$ (where X_{CH_4} is the fraction of unoccupied clathrate-lattice cages) and $T = 270\text{K}$ (worst case for CH₄ loss) yields $8 \times 10^{-16} \text{ m}^2 \text{ s}^{-1}$. In this case, 3 Gyr will allow approximately 10m of clathrate to be de-methanated by CH₄ loss, which is not important for our purposes. Plausible increases²⁰ to $10^{-14} \text{ m}^2 \text{ s}^{-1}$ do not alter this qualitative conclusion. CH₄ clathrate that is moved out of the P-T range of CH₄-clathrate stability will outgas CH₄ geologically quickly¹⁰⁷.

We calculate CH₄-clathrate stability assuming that thermal equilibrium is reached at each 1 Kyr timestep. This is reasonable because the depth of clathrate destabilization in our model is $\lesssim 250\text{m}$. Tests using a 1D scheme (tracking temperature as a function of depth) showed no qualitative difference in behavior. The latent heat of clathrate dissociation is ignored; this is acceptable because the thermal forcing of interest (from orbital variations) varies slowly compared to the speed of lowering of the clathrate table with or without latent-heat buffering. Geothermal heat flux is 0.03 W m^{-2} . The model is spun up with zero clathrate release for 5 Myr.

Regolith density (on top of the HSZ) is 2000 kg m^{-3} . A surface layer of 44m of ice (density 910 kg m^{-3}) is assumed poleward of 30° for $\varphi < 40^\circ$ (ref. 24). When $\varphi > 40^\circ$, this ice sublimates at 0.3 cm yr^{-1} . 3D climate models predict faster sublimation¹⁰⁸; however, faster sublimation rates would have no effect on our conclusions. We do not include thermal buffering from this icy material, but this would only slightly delay/damp the thermal wave. Ice-overburden sublimation tends to enhance and extend the atmosphere CH₄-enrichment episode in our model. To show that ice-overburden sublimation is not required for a CH₄ burst, the results of a high- φ to low- φ obliquity transition are shown in Fig. S5. In this simulation ice unloading does not occur (because nontropical ice is always unstable), and methane bursts still result.

CH₄-clathrate stability zone boundaries are taken from Table 4.1 of ref. 18. Destabilized CH₄ is assumed to be released to the atmosphere during the same timestep. Rapid release is a reasonable approximation because the thermal pulses are at orbital

frequencies (10^5 - 10^6 yr), and – especially when fracturing associated with clathrate destabilization is taken into account – CH_4 is unlikely to be trapped for this long. Once released, CH_4 is not recharged.

We evaluated additional CH_4 release from taliks beneath lakes. Sub-talik CH_4 release is initialized once atmospheric CH_4 exceeds an arbitrary, but radiatively reasonable threshold of 10^2 kg m^{-2} . We take this threshold to mark the onset of lake flooding. The warming-front depth is set to $2.32\sqrt{(\kappa\tau)}$ where $\kappa = 10^{-6} \text{ m}^2 \text{ s}^{-1}$ is thermal diffusivity and τ is time since sub-talik release is initialized. f beneath lakes is the same as f elsewhere. All CH_4 above the warming-front is released to the atmosphere. The warming-front's progress is halted at a depth 350 m, corresponding to pressure-stabilization of CH_4 -clathrate at $\sim 273\text{K}$. For a talik area of $1.1 \times 10^6 \text{ km}^2$ (corresponding to the Eridania paleolake; ref. 35), the talik feedback is minor compared to feedback release of CH_4 from un-inundated locations. However, if the flooded area was larger^{36,109}, talik feedback could be important.

CH_4 Destruction Parameterization.

We used the Caltech/JPL 1-Dimensional Mars photochemistry code, modified to include reduced C species^{23,110-111}. Estimated 2.7 Ga photon fluxes are used²⁶; our results would remain qualitatively the same for photon fluxes corresponding to times < 3.8 Ga. Boundary conditions include surface burial of O_2 , O_3 , H_2O_2 , and CO . H_2O is set to a specified mixing ratio at the surface, is well mixed up to the saturation altitude, follows the saturation vapor pressure until the atmosphere (by assumption) becomes isothermal, and becomes well mixed again above that. Results are insensitive to the specified H_2O surface-mixing ratio. The model is initialized with a specified amount of CH_4 . This initial CH_4 , and the (fixed) CO_2 abundance, were both varied. Results are shown in Figs. S3-S4. Atmospheric H_2 levels rise as CH_4 is destroyed, but the radiative effect of this H_2 is minor compared to CH_4 assuming the H_2 - CH_4 - CO_2 CIA parameterization of ref. 22.

At the CH_4/CO_2 ratios that are most relevant for this study (~ 0.005 - 0.02), CH_4 destruction rate is a function of CO_2/CH_4 ratio. This can be simply interpreted as the result of competition between CO_2 and CH_4 for UV photons: because CH_4 photolysis cross section is $\sim 10^2 \times$ that of CO_2 near Lyman- α wavelengths ($\sim 121.6 \text{ nm}$), CO_2 increasingly shields CH_4 from destruction as CH_4/CO_2 ratio decreases. At CH_4/CO_2 ratios that are less relevant for our climate scenario, more complicated behavior emerges. As expected¹¹², $\text{CH}_4/\text{CO}_2 > \sim 0.1$ leads to significant quantities of higher hydrocarbons and these could form an antigreenhouse haze. Because the model does not track production of hydrocarbons with mass greater than C_2H_6 , we do not attempt to track haze formation. For our $\text{CH}_4/\text{CO}_2 = 0.1$ runs, autocatalysis¹¹³⁻¹¹⁴ can play a significant role in CH_4 loss. For $\text{CH}_4/\text{CO}_2 < 0.005$, path dependence can be important, in that the secondary products of a high CH_4/CO_2 pulse interact with the H and H-species (like OH) produced by destruction

of the remainder of the CH₄^{xxx}. This appears to be the cause of the scatter at low values of CH₄/CO₂ in Figure S4.

The results are insensitive to varying the water volume-mixing ratio from 1 ppm to saturation at the surface. Results are sensitive to varying stratospheric diffusivity K_{zz} because K_{zz} regulates supply of CH₄ from the shielded lower atmosphere to the region of UV photolysis. For {pCO₂ = 500 mbar, pCH₄ = 1 mbar}, increasing K_{zz} by a factor of 100 reduces CH₄ lifetime by a factor of 8. This remains consistent with geologic constraints, and 100× the nominal K_{zz} profile is already pushing the limits on estimates of K_{zz} in the Martian atmosphere. To test sensitivity to photon flux, we first set K_{zz} to 100× nominal. Then, varying Ly- α , we found that the time-to-halving of initial CH₄ concentration scaled approximately as (flux)^{-0.8}. The photon-flux dependence is likely itself dependent on CH₄ concentration. Ly- α flux as a function of star age can be estimated using

$$I_{1216} = (3.7 \times 10^{-11} \text{ cm}^{-2} \text{ s}^{-1}) \times t_{\text{Gyr}}^{-0.72} / 4.56^{-0.72} \quad (4)$$

where t_{Gyr} is time after Mars formation in Gyr¹¹⁶. Plausible variations in this scaling could affect UV flux by a factor of several¹¹⁷.

The ancient destruction of atmospheric CH₄ at high pCH₄ (Figs. S3-S4) proceeds differently to destruction of CH₄ at low pCH₄ (e.g., modern Mars). At low pCH₄, roughly half of CH₄ loss is accounted for²⁵ by reactions between methane and oxidizing agents from photolysis of H₂O and CO₂. These reactions become less important as pCH₄ increases.

We did not find plausible parameter combinations for which CH₄ lifetime is <10 Kyr. Therefore, it is reasonable to infer on the basis of these results that the validity of the methane burst scenario depends on the size of the methane burst supplied to the atmosphere. If a burst is large enough to alter lake hydrology, then CH₄ destruction will be slow enough to match the lake-lifetime constraints.

Data availability.

The materials that support the findings of this study and the figures in this paper, including computer code, are available from the corresponding author upon request.

Methods-only references.

50. Fassett, C.I., Head, J.W. The timing of martian valley network activity: Constraints from buffered crater counting. *Icarus* **195**, 61-89 (2008).
51. Grant, J.A., Wilson, S.A. Late alluvial fan formation in southern Margaritifer Terra, Mars. *Geophys. Res. Lett.* **38**, L08201 (2011).
52. Grant, J.A., Wilson, S.A., Mangold, N., Calef, F., Grotzinger, J.P. The timing of alluvial activity in Gale crater, Mars. *Geophys. Res. Lett.* **41**, 1142-1149 (2014).

53. Mangold, N., Quantin, C., Ansan, V., Delacourt, C., Allemand, P. Evidence for Precipitation on Mars from Dendritic Valleys in the Valles Marineris Area. *Science* **305**, 78-81 (2004).
54. Mangold, N., Adeli, S., Conway, S., Ansan, V., Langlais, B. 2012. A chronology of early Mars climatic evolution from impact crater degradation. *J. Geophys. Res. - Planets* **117**, E04003.
55. Howard, A.D., Moore, J.M. 2011. Late Hesperian to early Amazonian midlatitude Martian valleys: Evidence from Newton and Gorgonum basins. *J. Geophys. Res. - Planets* **116**, E05003.
56. Warner, N., Gupta, S., Kim, J.-R., Lin, S.-Y., Muller, J.-P. Hesperian equatorial thermokarst lakes in Ares Vallis as evidence for transient warm conditions on Mars. *Geology* **38**, 71-74 (2010).
57. Wilson, S.A., A.D. Howard, J.M. Moore, J.A. Grant, A Cold-Wet Mid-Latitude Environment on Mars during the Hesperian-Amazonian Transition: Evidence from Northern Arabia Valleys and Paleolakes, *J. Geophys. Res. Planets* **121**, 1667-1694 (2016).
58. Werner, S.C., Tanaka, K.L. Redefinition of the crater-density and absolute-age boundaries for the chronostratigraphic system of Mars. *Icarus* **215**, 603-607 (2011).
59. Robbins, S.J, New crater calibrations for the lunar crater-age chronology. *Earth and Planetary Science Letters* **403**, 188-198 (2014).
60. Goudge, T.A.; Fassett, C.I.; Head, J.W.; Mustard, J.F.; Aureli, K.L., Insights into surface runoff on early Mars from paleolake basin morphology and stratigraphy. *Geology* **44**, 419-422 (2016).
61. Grant, J.A., Wilson, S.A. A possible synoptic source of water for alluvial fan formation in southern Margaritifer Terra, Mars. *Planet. Space Sci.* **72**, 44-52 (2012).
62. Adeli, S.; et al. Amazonian-aged fluvial system and associated ice-related features in Terra Cimmeria, Mars. *Icarus* **277**, 286-299 (2016).
63. Lamb, M.P.; Dietrich, W.E.; Aciego, S.M.; DePaolo, D.J.; Manga, M., Formation of Box Canyon, Idaho, by Megaflood: Implications for Seepage Erosion on Earth and Mars. *Science* **320**, 5879, 1067- (2008).
64. Hauber, E., et al. 2013. Asynchronous formation of Hesperian and Amazonian-aged deltas on Mars and implications for climate. *J. Geophys. Res. - Planets* **118**, 1529-1544.
65. Kite, E.S., Michaels, T.I., Rafkin, S., Manga, M., Dietrich, W.E. 2011, Localized precipitation and runoff on Mars. *J. Geophys. Res. - Planets* **116**, E07002.
66. Williams, R.M.E., Malin, M.C. Sub-kilometer fans in Mojave Crater, Mars. *Icarus* **198**, 365-383 (2008).
67. Williams, R.M.E., et al. Evidence for episodic alluvial fan formation in far western Terra Tyrrhena, Mars. *Icarus* **211**, 222-237 (2011).
68. Syvitski, J. P. M.; Peckham, S. D.; Hilberman, R.; Mulder, T., Predicting the terrestrial flux of sediment to the global ocean: a planetary perspective. *Sedimentary Geology* **162**, 5-24 (2003).
69. Morgan, A.M., et al. Sedimentology and climatic environment of alluvial fans in the martian Saheki crater & comparison with terrestrial fans in the Atacama Desert. *Icarus* **229**, 131-156 (2014).

70. Dietrich, WE, et al. 2017, Fluvial gravels on Mars, in D. Tsutsumi and J.B. Laronne (Eds.) *Gravel-Bed Rivers: Processes and disasters*, Wiley.
71. Barnhart, C.J., Howard, A.D., Moore, J.M. Long-term precipitation and late-stage valley network formation: Landform simulations of Parana Basin, Mars. *J. Geophys. Res. - Planets* **114**, E01003 (2009).
72. Matsubara, Yo; Howard, Alan D.; Gochenour, J. Parker, Hydrology of early Mars: Valley network incision, *J. Geophysical Research: Planets* **118**, 1365-1387.
73. Hoke, M.R. T.; Hynek, B.M. Roaming zones of precipitation on ancient Mars as recorded in valley networks. *J. Geophys. Res.*, **114**, E8, CiteID E08002 (2009).
74. Ody, A., et al. Global investigation of olivine on Mars. *J. Geophys. Res. - Planets* **118**, 234-262 (2013).
75. Koeppen, W.C., Hamilton, V.E. 2008. Global distribution, composition, and abundance of olivine on the surface of Mars from thermal infrared data. *J. Geophys. Res. - Planets* **113**, E05001.
76. Hamilton, Victoria E.; Christensen, Philip R., Evidence for extensive, olivine-rich bedrock on Mars. *Geology* **33**, p.433 (2005).
77. Viviano-Beck, C.E., et al. 2014. Revised CRISM spectral parameters and summary products based on the currently detected mineral diversity on Mars. *J. Geophys. Res. - Planets* **119**, 1403-1431.
78. Ehlmann, B.L., Buz, J. 2015. Mineralogy and fluvial history of the watersheds of Gale, Knobel, and Sharp craters. *Geophys. Res. Lett.* **42**, 264-273.
79. Bullock, M.A.; Moore, J.M., Atmospheric conditions on early Mars and the missing layered carbonates, *Geophys. Res. Lett.* **34**, 19, CiteID L19201 (2007).
80. Hurowitz, Joel A.; McLennan, Scott M., 2007, A ~3.5 Ga record of water-limited, acidic weathering conditions on Mars, *Earth Planet. Sci. Lett.* **260**, Issue 3-4, p. 432-443.
81. Tosca, N.J., Knoll, A.H. Juvenile chemical sediments and the long term persistence of water at the surface of Mars. *Earth Planet. Sci. Lett.* **286**, 379-386 (2009).
82. Squyres, S.W., et al., Rocks of the Columbia Hills, *J. Geophys. Res. - Planets* **111**, Issue E2, CiteID E02S11 (2006).
83. Elwood Madden, M. E.; Madden, A. S.; Rimstidt, J. D., How long was Meridiani Planum wet? Applying a jarosite stopwatch to determine the duration of aqueous diagenesis. *Geology* **37**, 635-638 (2009).
84. Siebach, K.L., et al., Sorting out compositional trends in sedimentary rocks of the Bradbury group (Aeolis Palus), Gale crater, Mars, *J. Geophys. Res.* **122**, 295–328 (2017).
85. Woo, M.-K., 2012, *Permafrost Hydrology*, Springer.
86. Forget, F., Haberle, R.M., Montmessin, F., Levrard, B., Head, J.W. Formation of Glaciers on Mars by Atmospheric Precipitation at High Obliquity. *Science* **311**, 368-371 (2006).
87. Skinner, J.A., Tanaka, K.L., Platz, T. Widespread loess-like deposit in the Martian northern lowlands identifies Middle Amazonian climate change. *Geology* **40**, 1127-1130 (2012).
88. Irwin, R.P., III, 2013. Testing Links Between Impacts and Fluvial Erosion on Post-Noachian Mars, Lunar and Planetary Science Conference, LPI Contribution No. 1719, p.2958.

89. Ramirez, R.M.; Kasting, J.F. Could Cirrus Clouds Have Warmed Early Mars?, *Icarus*, **281**, 248-261 (2017).
90. Mumma, M.J.; Charnley, S.B., The Chemical Composition of Comets—Emerging Taxonomies and Natal Heritage. *Annu. Rev. Astron. Astrophys.* **49**, 471-524 (2011).
91. Laskar, J., Correia, A.C.M., Gastineau, M., Joutel, F., Levrard, B., Robutel, P. Long term evolution and chaotic diffusion of the insolation quantities of Mars. *Icarus* **170**, 343-364 (2004).
92. Chambers, J.E. A hybrid symplectic integrator that permits close encounters between massive bodies. *Monthly Notices Royal Astron. Soc.* **304**, 793-799 (1999).
93. Armstrong, J.C., Leovy, C.B., Quinn, T. A 1 Gyr climate model for Mars: new orbital statistics and the importance of seasonally resolved polar processes. *Icarus* **171**, 255-271 (2004).
94. Li, G., Batygin, K. On the Spin-axis Dynamics of a Moonless Earth. *Astrophys. J.* **790**, 69 (2014).
95. Lissauer, J.J., Barnes, J.W., Chambers, J.E. Obliquity variations of a moonless Earth. *Icarus* **217**, 77-87 (2012).
96. Fastook, James L.; Head, James W., Glaciation in the Late Noachian Icy Highlands: Ice accumulation, distribution, flow rates, basal melting, and top-down melting rates and patterns, *Planetary and Space Science* **106**, 82-98. (2015)
97. Mahaffy, P.R., et al. The imprint of atmospheric evolution in the D/H of Hesperian clay minerals on Mars. *Science* **347**, 412-414 (2015).
98. Mousis, O., et al. 2013. Volatile Trapping in Martian Clathrates. *Space Science Reviews* **174**, 213-250.
99. Mousis, O., et al. Methane Clathrates in the Solar System. *Astrobiology* **15**, 308-326 (2015).
100. McCollom, T.M., Formation of meteorite hydrocarbons from thermal decomposition of siderite, *Geochim. Cosmochim. Acta* **67**, 311-317.
101. Tréhu, A.M.; et al. 2014, Feeding methane vents and gas hydrate deposits at south Hydrate Ridge, *Geophys. Res. Lett.*, **31**, CiteID L23310.
102. Besserer, J., F. et al. (2014), GRAIL gravity constraints on the vertical and lateral density structure of the lunar crust, *Geophys. Res. Lett.* **41**, 5771–5777 (2014).
103. Onstott, T.C., et al. Martian CH₄: Sources, Flux, and Detection. *Astrobiology* **6**, 377-395 (2006).
104. Klauda, J.B., and Sandler, S.I., 2005, Global Distribution of Methane Hydrate in Ocean Sediment, *Energy Fuels*, **19** (2), 459–470.
105. Levi, A.; Sasselov, D.; Podolak, M., Structure and Dynamics of Cold Water Super-Earths: The Case of Occluded CH₄ and Its Outgassing, *Astrophys. J.* **792**, 2, article id. 125, 44 pp. (2014).
106. Peters, B., Zimmermann, N.E.R., Beckham, G.T., Tester, J.W., Trout, B.L., Path sampling calculation of methane diffusivity in natural gas hydrates from a water-vacancy assisted mechanism. *J. Am. Chem. Soc.* **130**, 17,342–17,350 (2008).

107. Stern, L.A., Circone, S., Kirby, S.H., Durham, W.B. 2003. Temperature, pressure, and compositional effects on anomalous or "self" preservation of gas hydrates. *Canadian J. Phys.* 81, 271-283.
108. Madeleine, J.-B., et al. Amazonian northern mid-latitude glaciation on Mars: A proposed climate scenario. *Icarus* **203**, 390-405 (2009).
109. Carr, M.H., Head, J.W. Oceans on Mars: An assessment of the observational evidence and possible fate. *J. Geophys. Res. - Planets* **108**, 5042-1 (2003).
110. Summers, M.E.; Lieb, B. J.; Chapman, E.; Yung, Y.L., Atmospheric biomarkers of subsurface life on Mars, *Geophys. Res. Lett.* **29**, 24-1, CiteID 2171 (2002).
111. Nair, Hari; Allen, Mark; Anbar, Ariel D.; Yung, Yuk L.; Clancy, R. Todd, A photochemical model of the martian atmosphere, *Icarus* **111**, 124-150 (1994).
112. Wong, Ah-San; Atreya, Sushil K.; Encrenaz, Thérèse, 2003, Chemical markers of possible hot spots on Mars, *J. Geophys. Res. - Planets*) **108**, CiteID 5026 (2003).
113. Allen, M.; Yung, Y. L.; Pinto, J. P., Titan - Aerosol photochemistry and variations related to the sunspot cycle, *Astrophys. J.* **242**, L125-L128 (1980).
114. Yung, Y. L.; Allen, M.; Pinto, J. P., Photochemistry of the atmosphere of Titan - Comparison between model and observations, *Astrophysical Journal Supplement Series* **55**, 465-506 (1984).
115. McKay, Christopher P.; Pollack, James B.; Courtin, Regis, The greenhouse and antigreenhouse effects on Titan, *Science* **253**, 1118-1121 (1991).
116. Ribas, I., Guinan, E.F., Güdel, M., Audard, M. Evolution of the Solar Activity over Time and Effects on Planetary Atmospheres. I. High-Energy Irradiances. *Astrophys. J.* **622**, 680-694 (2005).
117. Tu, L.; Johnstone, C.P.; Güdel, M.; Lammer, H., The extreme ultraviolet and X-ray Sun in Time: High-energy evolutionary tracks of a solar-like star. *Astron. Astrophys.* **577**, article L3, 4 pp. (2015).

SI Guide

Supplementary Figures and Supplementary Table

pdf format, 2.8 MB.

The Supplementary Figures show:

- (1) An olivine outcrop in an alluvial fan source region
- (2) Clathrate charge-up and release scenario
- (3) Methane drawdown curves varying initial pCH₄ and pCO₂
- (4) Methane destruction rates plotted against CH₄/CO₂ ratio
- (5) Detailed results for different CH₄-release scenarios.

The Supplementary Table shows minimum lake lifetimes obtained for 6 Mars deltas.

Supplementary Information.

Site	Delta volume (V_d , km ³)	Lake area (A_p , km ²)	Evaporation rate constraint (E , m/yr)	V_w/V_s assumed	Minimum lake lifetime (Kyr)
Eberswalde delta (1)	6	>410	<1 m/yr	10 ³	15
SW Melas Fan "C" (2)	3.5	350	<1 m/yr	10 ³	10
SW Melas Fan "F" (2)	1.3	350	<1 m/yr	10 ³	4
Dulce Vallis (3)	1.5	3008	<1 m/yr	10 ³	0.5
Farah Vallis (4)	22.5	3617	<1 m/yr	10 ³	6
Gale Pancake (3)	14	5832	<1 m/yr	10 ³	3

Sources of measurements: 1. Irwin et al. 2015. 2. Williams & Weitz 2014. 3. Palucis et al. 2016.

Table S1. Minimum paleolake lifetimes. We used published delta volume and lake area data, and applied a uniform lake evaporation rate and sediment:water ratio.

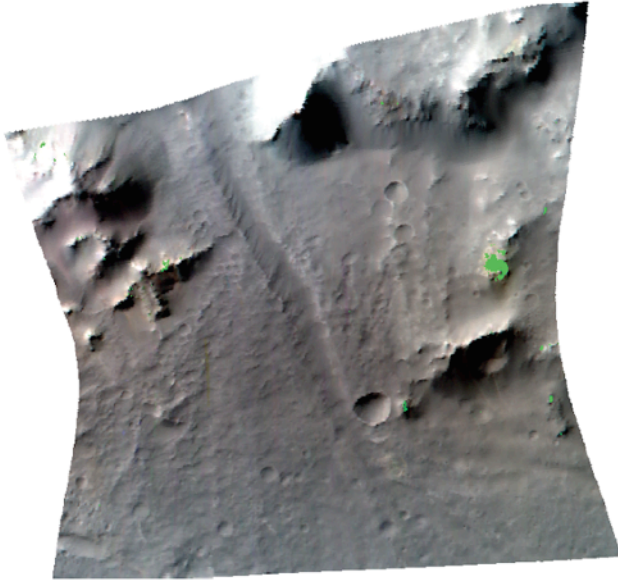


Fig. S1. An olivine outcrop in an alluvial fan source region (fan drains to bottom of image). Olivine detections highlighted in green. Spectra for individual pixels within these areas were checked manually in order to verify that absorptions diagnostic of olivine were present. CRISM FRT00016E79, Saheki crater. Work by David P. Mayer.

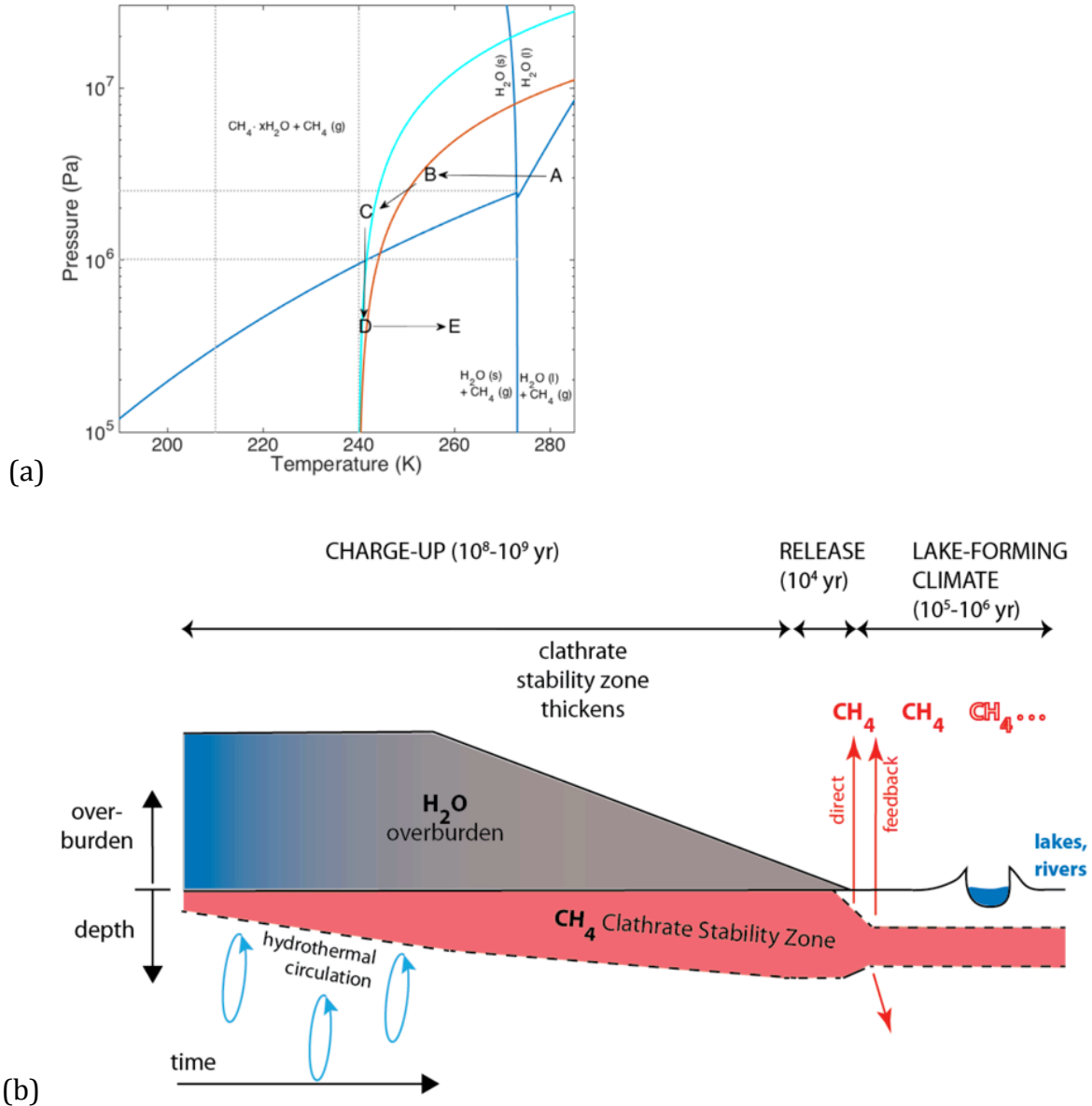


Fig. S2. Clathrate charge-up and release scenario. **(a)** Methane clathrate phase diagram, showing pathways to charge-up and release. Phase boundaries shown in dark blue. Mars geotherms shown in red (early, steep geotherm) and cyan (later, shallow geotherm). Early in Mars history, cooling of the geotherm locks-in CH_4 as clathrate in regolith, e.g. beneath early seas or ice sheets (A \rightarrow B). Further geotherm cooling and escape of ice-sheet water to space (B \rightarrow C) has little effect on CH_4 -clathrate stability. Orbital change drives ice shift which leads to CH_4 breakdown (C \rightarrow D). Orbitaly-induced warming of the surface, plus warming induced by earlier release of CH_4 , move the regolith deeper into the CH_4 -clathrate destabilization region (D \rightarrow E). (In practice, steps C \rightarrow D and D \rightarrow E overlap). **(b)** Schematic of the long-term evolution of a column of the Mars uppermost crust.

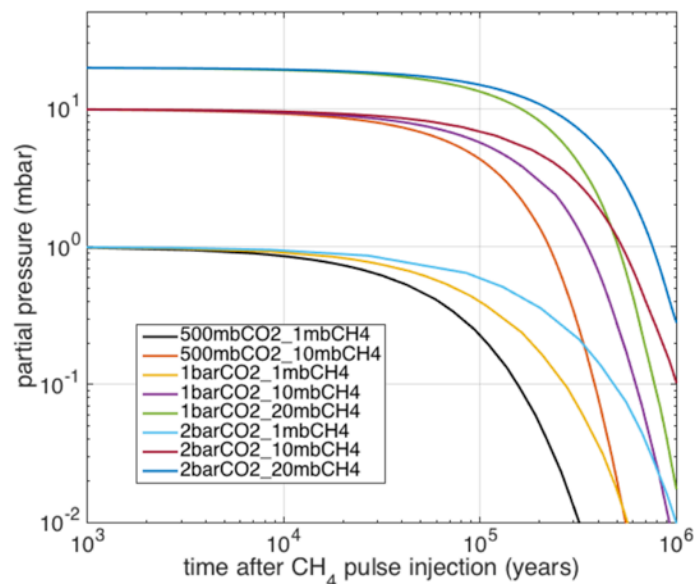


Fig. S3. Methane drawdown for initial methane concentrations of 1mb, 10mb, and 20mb, in CO₂ atmospheres of varying thickness. The 500 mb CO₂, 20 mb CH₄ case is not shown due to numerical instability.

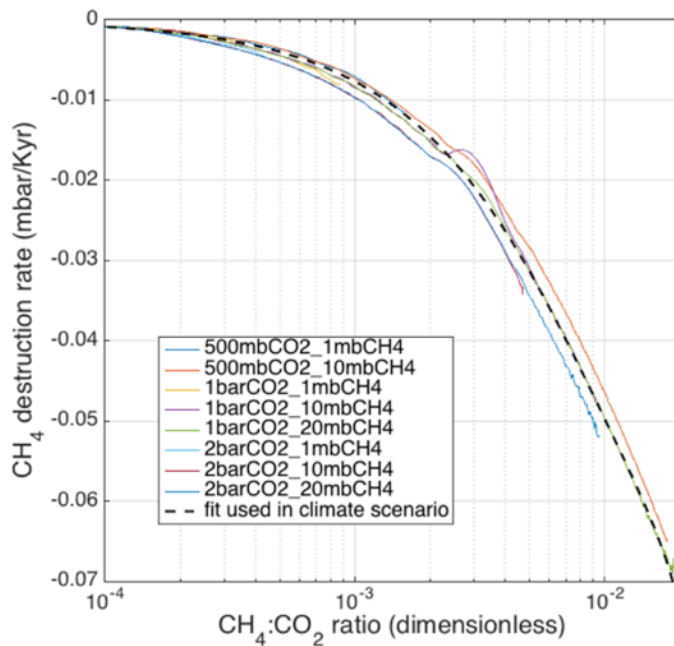
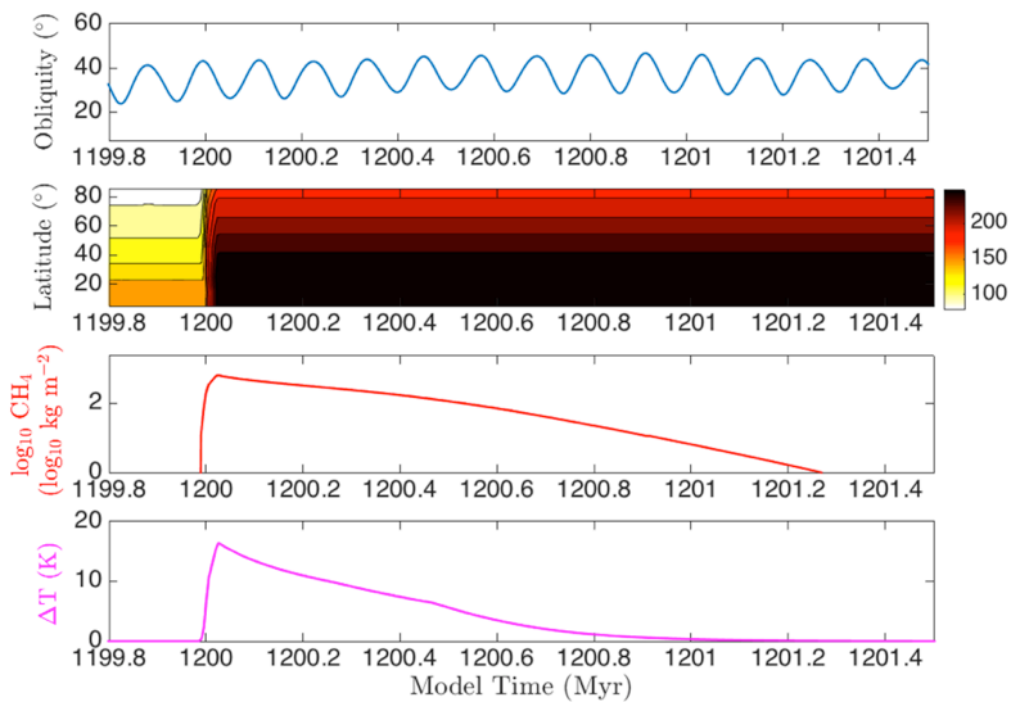
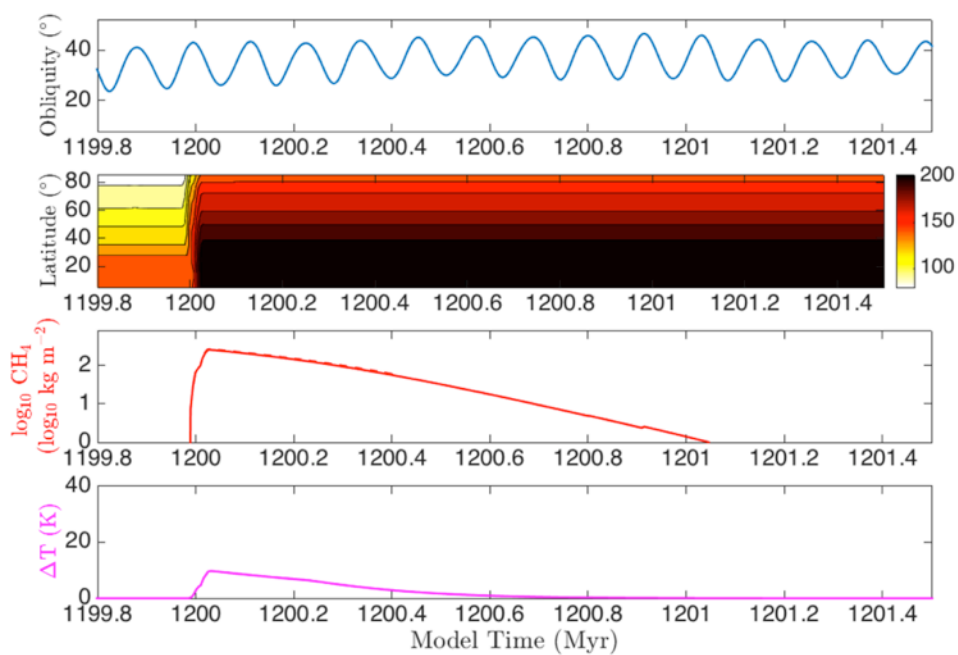


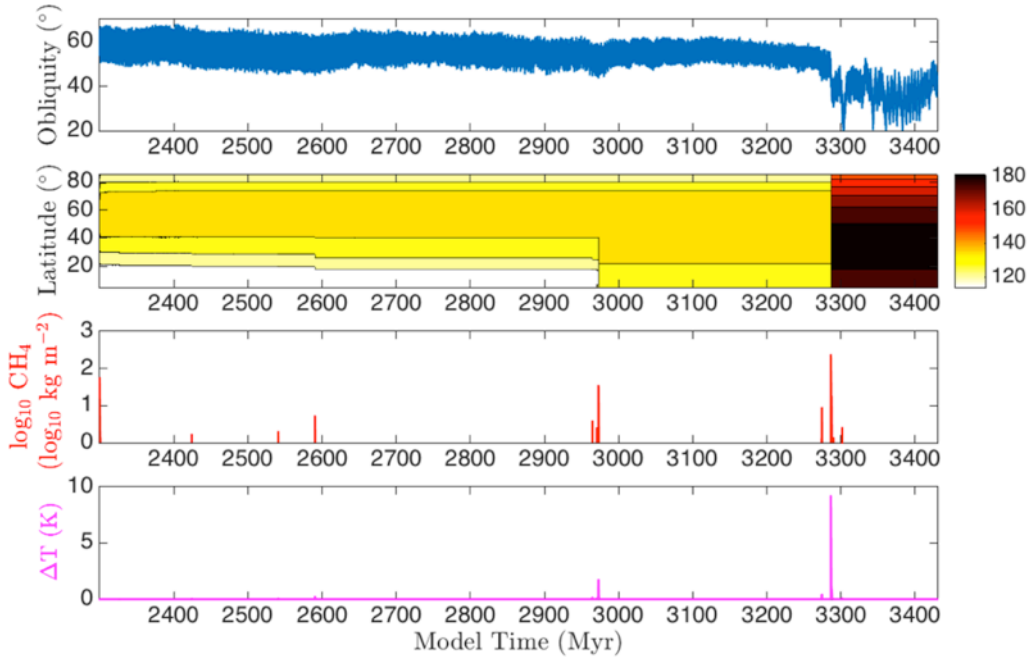
Fig. S4. Methane destruction rate. The first 15 Kyr of each run are excluded due to numerical artifacts associated with model startup. The dashed black line is a fit to the 1 bar CO₂, 20 mbar CH₄ run.

(a)

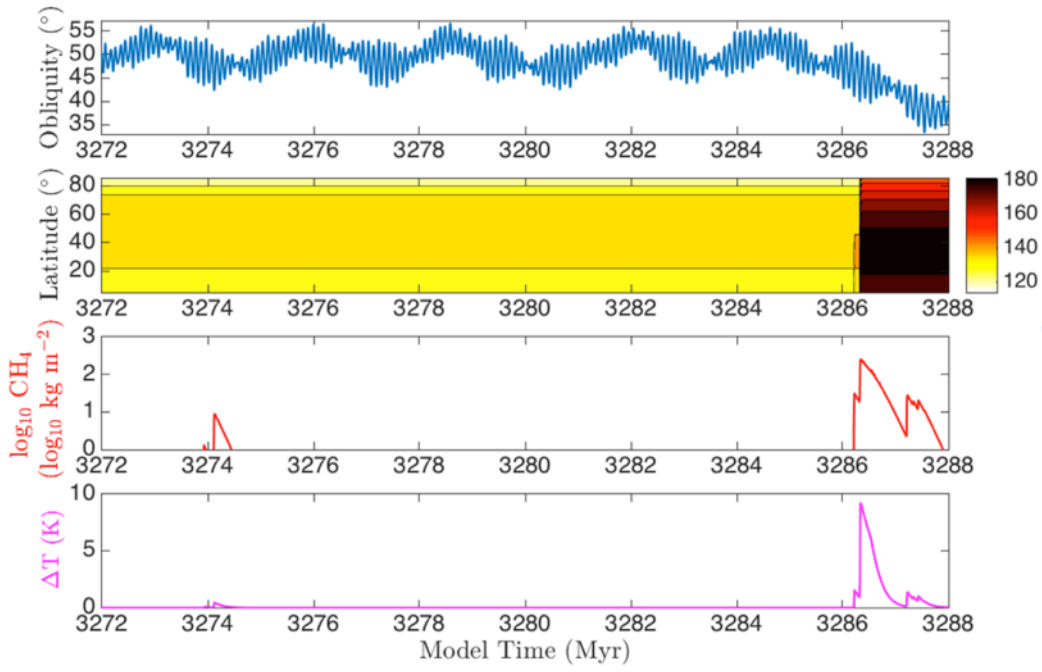


(b)





(c)
(d)



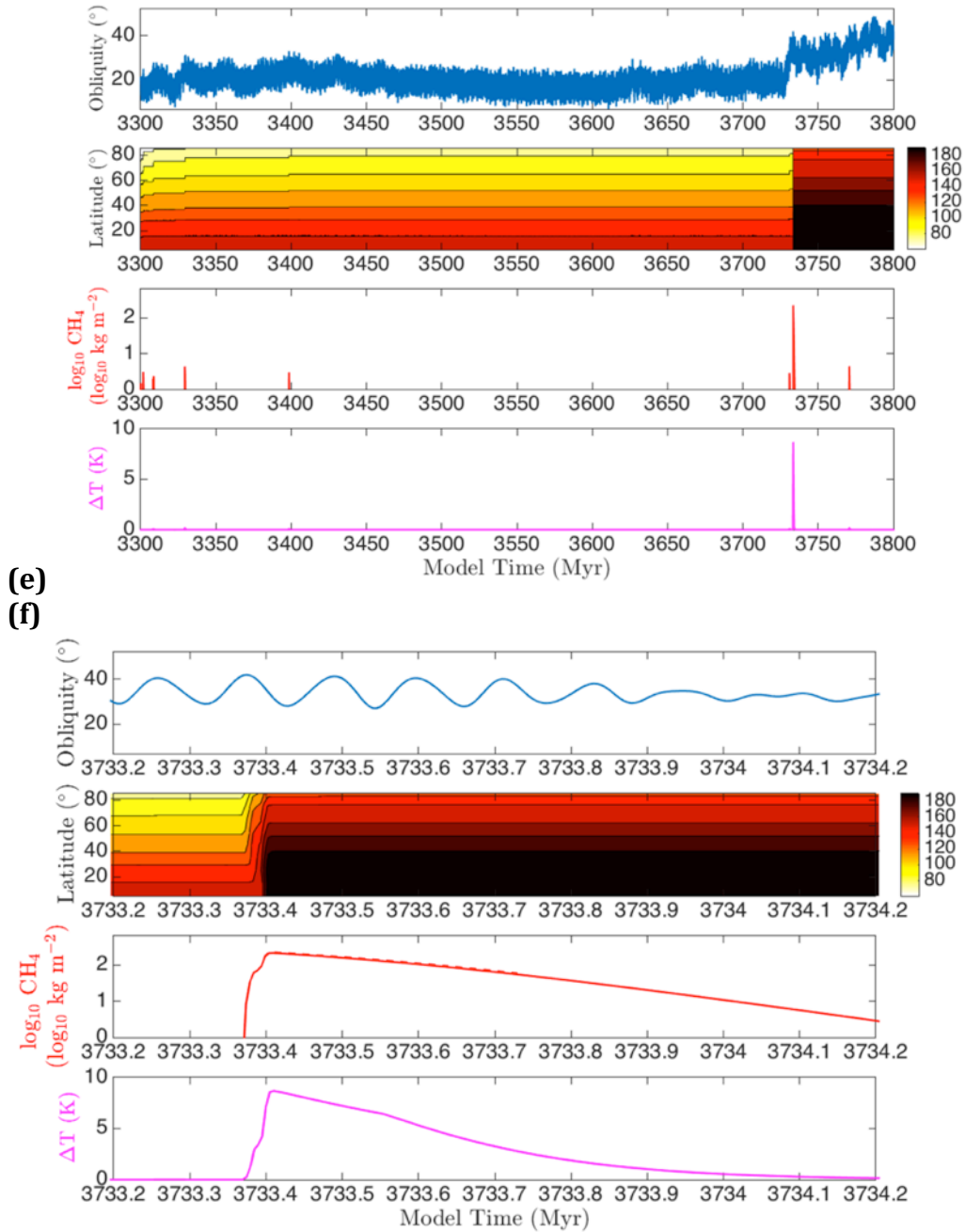


Fig. S5. Different CH_4 -release scenarios. Model time is arbitrary. For each subfigure, the top panel shows example obliquity forcing. The colors in the second panel show the depth to the top of the clathrate-hydrate stability zone (depth in meters). Darkening of colors indicates clathrate destabilization. The third panel shows atmospheric CH_4 column mass. Dashed line includes talik feedback. The bottom panel shows temperature change. Solid line is for CH_4 alone; dashed line is for $\text{CH}_4 + 10\% \text{C}_2\text{H}_6$. (a) Zoom in on the biggest CH_4 burst from the $f = 0.045$ simulation shown in Fig. 4. (b) As for (a), but with $f = 0.03$, showing strong sensitivity to f . (c) CH_4 bursts for a simulation of long-term φ decline (temperature effects only, no decompression); $f = 0.045$. (d) Zoom in on part of

(c). (e) Showing a different φ -rise scenario, with $f = 0.03$ (compare to Fig. 4). (f) Zoom in on the biggest CH_4 burst from the simulation shown in (e).